Structure and dynamics of ionic borate glasses

C. P. E. Varsamis,[1] *A. Vegiri & E. I. Kamitsos*

Theoretical and Physical Chemistry Institute, The National Hellenic Research Foundation, 48 Vass. Constantinou Ave., 116 35 Athens, Greece

The structural and dynamic properties of ionic borate glasses with composition xM_2O–$(1-x)B_2O_3$ (M=Li, Cs) are revisited in view of recent results of molecular dynamics simulations. Simulations were carried out in collections of ~512 atoms in the canonical ensemble for compositions $0{\cdot}20 \le x \le 0{\cdot}50$ and temperatures 300, 600 and 1250 K. The short range order structure of these glasses was found to depend on temperature and on the alkali oxide modifier content, as well as on the nature of the alkali ion. The structural trends resulted from simulations are compared with those derived from different experimental techniques. At the nanoscale size, it was possible to distinguish long lived and well distinguished network sites hosting alkali metal ions. The distribution of cations in the glassy network was found to be inhomogeneous and consistent with the predictions of the modified random network model. Cation dynamics were evaluated in both short and long time scales. In particular, the vibrational properties of cations were found to depend strongly on the nature of their hosting sites, whereas their diffusivity is facilitated by the presence of nonbridging oxygen (NBO) atoms. The detailed analysis of the ion transport mechanism revealed discrete hopping of ions mostly between similar neighbouring sites. The calculated cluster size distribution curves for cations and NBO atoms were found to obey the predictions of percolation theory. The formation of percolating clusters above a certain composition threshold supports strongly the existence of a percolating diffusion mechanism for ionic borate glasses.

Introduction

Ionic borate glasses are characterised by the continuous non-monotonic variation of their structural, dynamic and macroscopic properties with increasing the modifier oxide content. This phenomenon, known as the "borate anomaly" effect, has been the subject of numerous investigations.[1] The detailed knowledge of the dependence of their structural and dynamic aspects on composition is highly desirable in order to correlate them with their macroscopic properties. The establishment of such correlations is of great importance since these materials have potential applications in electrochemical devices.[2]

The structural properties of ionic borate glasses have been extensively investigated over the years. Early experimental studies including infrared,[3] NMR[4–6] and Raman[7] investigations concluded that the structure of vitreous B_2O_3 consists of neutral $B\emptyset_3$ triangles found in random configurations and in B_3O_6 boroxol ring formations ($\emptyset$ denotes an oxygen atom bridging two boron centres). Addition of alkali oxide content to vitreous B_2O_3 results in the progressive transformation of borate triangles into charged tetrahedral entities, $B\emptyset_4^-$.[3–7] It was further suggested that in alkali borate glasses, xM_2O–$(1-x)B_2O_3$ (M=alkali ion), for compositions with $x<0{\cdot}30$ the fraction N_4 of tetrahedral units follows the $N_4=x/(1-x)$ law.[4–6] For higher compositions, there is the progressive depolymerisation of the borate network by the formation of charged triangles with nonbridging oxygen (NBO) atoms, like metaborate, $B\emptyset_2O^-$, pyroborate, $B\emptyset O_2^{2-}$, and orthoborate, BO_3^{3-} triangles.

Despite the fact that the aforementioned structural mechanisms in ionic borate glasses are widely accepted, thus providing the basis for the explanation of the "borate anomaly", the dependence of the short range order (SRO) structure on the nature of the modifier ion is still a controversial issue. On one hand, early NMR studies concluded that the SRO structure has no dependence on the alkali type[4–6] while on the other, a plethora of early experimental measurements including viscosity,[8] absorption edge[9] optical basicity,[10,11] glass transition temperature, thermal expansion coefficient,[12,13] as well as sound velocity and elastic constant measurements[14,15] showed the clear dependence of the SRO structure on the nature of the alkali modifier. Along the same lines, spectroscopic investigations employing ^{11}B NMR,[16] Raman,[17] infrared,[18] DAS NMR[19] and neutron scattering, as well as molecular dynamics simulations[21–23] provided also to the dependence of the SRO structure on the type of the alkali ion. The controversy is still going on, since recent ^{11}B MAS-NMR investigations concluded that the type of alkali metal does not affect the network structure,[24,25] thus leaving this issue open for further investigations.

Besides the SRO network structure, an equally important structural aspect is the identification of

[1] Corresponding author. Email: cvars@eie.gr

the local structures hosting the metal cations and the knowledge of cation site interactions in borate glasses. Early ideas, based on the continuous random network model proposed by Zachariasen[26] and applied to alkali silicate glasses by Warren & Biscoe,[27,28] suggested the homogeneous distribution of alkali metal ions in voids or sites of the silicate network. On the contrary, on the basis of EXAFS studies in sodium silicate glasses, Greaves proposed the inhomogeneous distribution of metal ions in the silicate network, i.e. the so-called modified random network model.[29]

In ionic borate glasses, early studies suggested that metal ions are not homogeneously distributed in the glassy network.[30–33] Further evidence for structural inhomogeneity at the nanoscale size was provided by far infrared spectroscopy since vibrations of metal ions in their hosting sites are active in the far infrared region.[34–36] In borate glasses, as well as in most ionic glasses, the asymmetric far infrared profiles showed the existence of at least two distinct environments of cation hosting sites.[37–41] The so-called "two site" model has been initially attributed to the ability of the borate network to provide cation hosting sites with variable charge density and coordination number.[39] In a different viewpoint, however, the far infrared absorption of sodium borate glasses was assigned to vibrational modes of Na ions in a single type of hosting sites.[42] Differently again, Wright and coworkers concluded that the rigidity of borate superstructural units along with the lack of periodicity in the glass structure should lead normally to a considerable variation of cation hosting sites in terms of site distortion and coordination numbers.[43]

It is clear from the aforementioned discussion that the microstructure of borate glasses and the nature and distribution of metal ion hosting sites as well as their spatial distribution constitute an issue of open discussion. At the same time, this information is particularly valuable towards a better understanding of transport properties in ionic glassy materials. In fact, different models for ionic transport in glasses proposed so far involve, in general, the nature and distribution of metal ion hosting sites. For example, theoretical studies of the ionic conductivity mechanism were based on the existence of distinct cation sites and preferred pathways for ion transport,[44] microsegregation of cations in channels suitable for ion migration,[29] or cation site memory effects.[45] Moreover, recent approaches of the ion transport mechanism in single[46–48] or mixed[49] alkali glasses invoked the 'two site' model.

In the present manuscript we review recent results of molecular dynamics simulations in Li- and Cs-containing borate glasses. Emphasis is given on the dependence of the SRO structure on the composition, temperature and nature of the metal ion and the results are compared with experimental NMR and infrared findings. Then the microstructure of the metal ion hosting sites is investigated according to the type of structural borate unit with which they interact primarily. Moreover, we explore the possibility to distinguish different types of cations according to the particular environment in which they predominantly reside. This information is further elaborated to calculate the dynamic responses of ions in both the short and long time regime. Finally, we report also on the ionic conductivity mechanism based on the spatial distribution of cations in the glassy network and on their dynamical responses. The results are discussed in the framework of existing experimental or theoretical dynamic studies of ionic borate glasses.

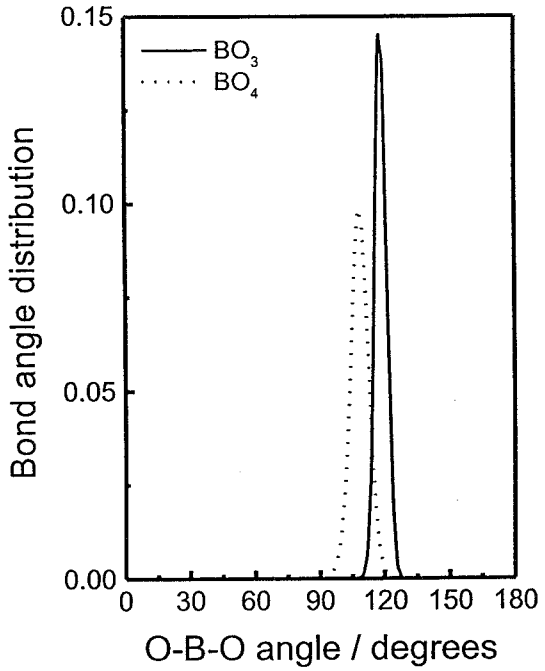

Figure 1. Distribution function of O–B–O angles for glass $0{\cdot}3Li_2O.0{\cdot}7B_2O_3$ at T=300 K

Computational details

Molecular dynamics simulations were performed for xM_2O–$(1-x)B_2O_3$ glasses, with x=0·2–0·6 for M=Li and x=0·2–0·4 for M=Cs, and temperatures 300 K and 1250 K. Structures consisting of ~256 atoms (M=Li) and ~512 atoms (M=Cs) in a primitive cubic cell have been generated. For each composition, we used appropriate speciation of atoms whereas the lattice constant of the cubic cell was determined from experimental density data, as reported in detail in Ref. 50. The interaction potential was of the usual Born–Mayer–Huggins form augmented by an additional three-body harmonic interaction term for the O–B–O angles. We have employed the potential form and the values of the relevant parameters reported previously,[51] where a partial screening of the electrostatic charges for B

and O atoms was found necessary for reproduction of experimental infrared and Raman spectra.

The simulations were carried out in the canonical ensemble with periodic boundary conditions, while long range Coulomb forces were handled by employing the Ewald summation method.[52] A fifth order Gear predictor–corrector integrator with a time step of 0·96 fs was used and the randomly generated melts at ~6000 K were quenched to the final temperature in five cooling cycles. Each cycle consisted of a fast cooling step of about 2 ps and an equilibration period of about 10 ps. The equilibration period in the final cooling cycle was 30 ps, whereas positions and velocities of each particle were accumulated for a final period of more than 180 ps in order to get reliable statistics for the diffusive ionic motion. Further details of the computational method can be found in Refs. 23, 50, 53.

Results and discussion

Short range order structure of Li- and Cs-containing borate glasses

The detailed mapping of the short range order structure of the glasses was determined by examining the B–O radial distribution functions, $g_{B\text{-}O}(R)$, at each glass composition and temperature investigated. Integration of these functions provides directly the average boron–oxygen coordination numbers, <B(O)>, from which it is possible to determine the molar fractions of the borate polyhedra. In doing so, we first examined the O–B–O angle distribution functions, a typical example of which is reported in Figure 1, for the $0{\cdot}3Li_2O$–B_2O_3 composition at T=300 K. As shown, these functions exhibit two sharp peaks at ~109·5° and 120° which are characteristic for the presence of tetrahedral and triangular borate units. It is also underlined that the profiles of these functions remain unaffected for each composition and temperature studied suggesting that borate tetrahedral and triangles constitute the only structural entities encountered in the present simulated glasses.

In order to quantify the SRO network structure, the molar fractions of tetrahedral borate units, X_4, were determined from the integration of the $g_{B\text{-}O}(R)$ functions by the expression X_4=<B(O)>−3. The results are depicted in Figure 2 for T=300 and 1250 K and compared with the theoretical curve $x/(1-x)$ and existing room temperature NMR data for Cs-[16,24] and Li-borate glasses.[16] As seen, simulated X_4 values are systematically lower than the experimental ones. This effect is attributed to the higher quenching rates of simulated glasses which result in the enhancement of the molar fractions of triangular units with nonbridging oxygen (NBO) atoms and, consequently, in lower X_4 values.[51,54,55] Inspection of Figure 2 shows that for the x=0·2 composition, room temperature simulated

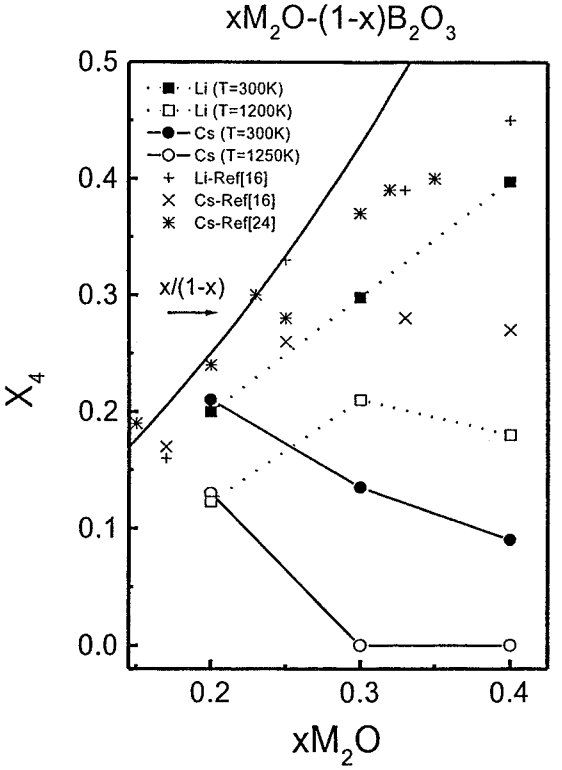

Figure 2. Molar fraction of $B\emptyset_4^-$ tetrahedral units, X_4, in simulated Cs- and Li-borate glasses as a function of composition and temperature. Experimental room temperature NMR data reported for Li-[16] and Cs-borate glasses[16,24] are also included. The x/(1−x) curve gives the X_4 value if $B\emptyset_4^-$ tetrahedra are the only charged units existing in borate glasses

X_4 values for Li- and Cs-borates are practically the same and present the smallest deviation from both NMR data and the theoretical $x/(1-x)$ value. This finding indicates that the effect of the cooling rate on the SRO structure becomes less pronounced whenever the fraction of NBO-containing units is small. This is in close agreement with a recent temperature Raman study of K-borate glasses which demonstrated that the Raman profiles of the x=0·3 glass/melt are much more sensitive to temperature changes than those of the x=0·2 glass/melt.[56]

For compositions with x=0·3, simulated X_4 values for Cs-borates are significantly lower than those for Li-containing glasses with the same alkali oxide content. This trend is consistent with the NMR data of Ref. 16 and is in contrast with those of Ref. 24. It is noted that differences in NMR data through the years have been attributed recently to variations in the quenching rates employed in different studies.[25] Within this context, it is underlined that the present simulations for Li and Cs-borate glasses were carried out under the same cooling procedure and, thus, whatever similarities (i.e. for x=0·2) or differences (for x≥0·3) were observed in the network structure between the two simulated glass systems cannot be

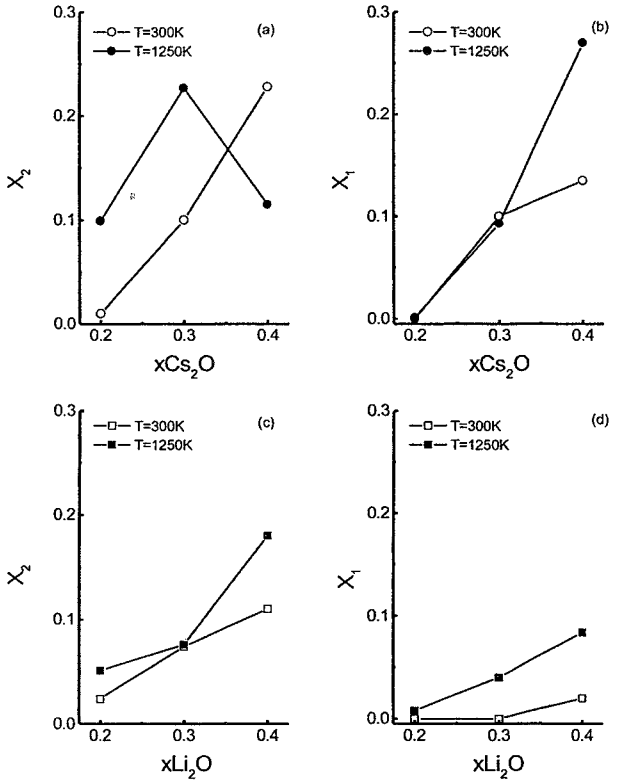

Figure 3. Molar fractions of $B\emptyset_2O^-$, X_2, and $B\emptyset O_2^{2-}$, X_1, units in simulated Cs- and Li-borate glasses as a function of alkali content and temperature

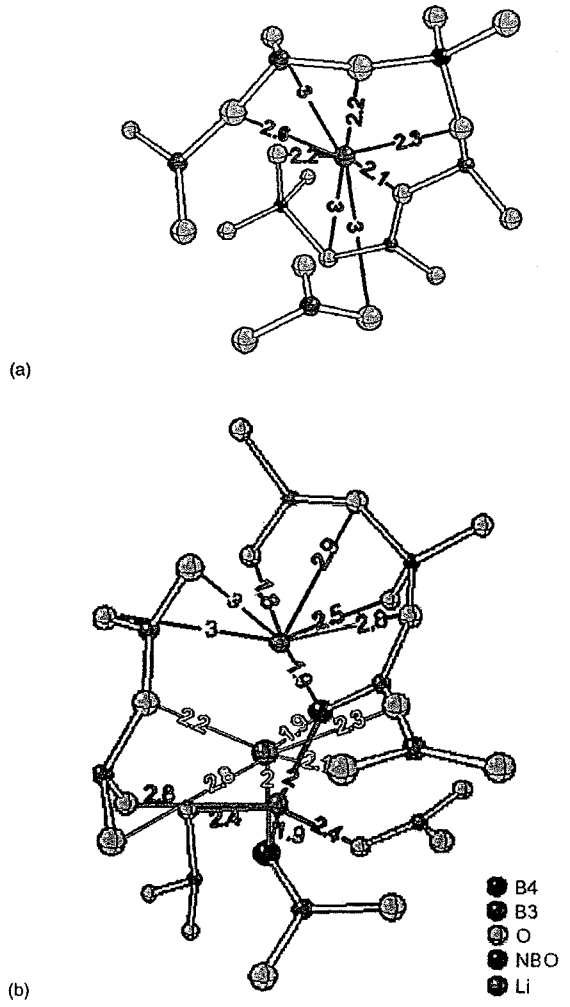

Figure 4. Simulated structures for Li hosting sites at T=300 K for the $0{\cdot}3Li_2O.0{\cdot}7B_2O_3$ glass: (a) b-type site, and (b) nb-type site. Distances between Li ions and oxygen atoms in the first coordination shell within a radius of 3 Å are included. B_4 and B_3 denote fourfold and threefold coordinated boron atoms while BO and NBO denote bridging and nonbridging oxygen atoms, respectively

attributed to cooling rate variations.

Deviations of X_4 values from the theoretical value $x/(1-x)$ indicate the presence of charged triangular borate units with NBO atoms. In order to determine their molar fraction, an oxygen atom was identified as nonbridging if no other boron atom was found in its vicinity within the first minimum of the B–O radial distribution curve. This minimum at ~2 Å was found to be independent of temperature and composition. This procedure provides the total number of NBO atoms, while the number of NBO atoms per charged triangular entity can be determined by their average charge evaluated from the integration of the first peak of the corresponding NBO–NBO correlation function, which gives the average number of NBOs seen by an NBO atom on the same unit.[50] The calculated molar fractions X_2 and X_1 for charged triangular borate units with one, $B\emptyset_2O^-$, or two NBO atoms, $B\emptyset O_2^{2-}$, respectively, are reported in Figure 3 for Li- and Cs-borate glasses at T=300 and 1250 K. As expected, for x=0·2 both systems have similar values while for higher compositions X_2 and X_1 are systematically enhanced in Cs-containing glasses.

The results reported in Figures 2 and 3 clearly show that the SRO structure depends on the temperature as well. In particular, for x=0·2, the temperature increase results in the transformation of $B\emptyset_4^-$ tetrahedral into charged $B\emptyset_2O^-$ triangular entities. Such a transformation can be fully described by invoking the following isomerisation reaction

$$B\emptyset_4^- \Leftrightarrow B\emptyset_2O^- \quad (1)$$

which shifts to the right with increasing temperature. This finding is fully consistent with the results of statistical mechanical calculations[57] and of spectroscopic NMR,[58,59] infrared,[41] x-ray diffraction[60] and Raman[56] investigations which showed that the NBO-containing triangular units of modified borate glasses are favoured at high temperatures at the expense of $B\emptyset_4^-$ tetrahedra.

For compositions higher than x=0·2, increasing temperature results in the conversion of $B\emptyset_4^-$ tetrahedra into $B\emptyset_2O^-$ and $B\emptyset O_2^{2-}$ units. The transformation into $B\emptyset_2O^-$ units is described with Equation (1) while the creation of $B\emptyset O_2^{2-}$ units may result from the fol-

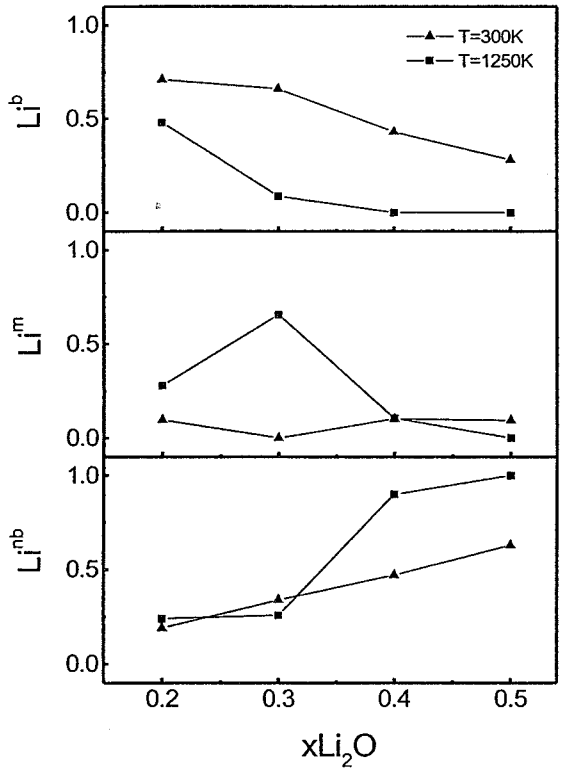

Figure 5. Molar fractions of Li metal ions in b-type, Li^b, nb-type, Li^{nb}, and mixed type, Li^m, environments. For details see text

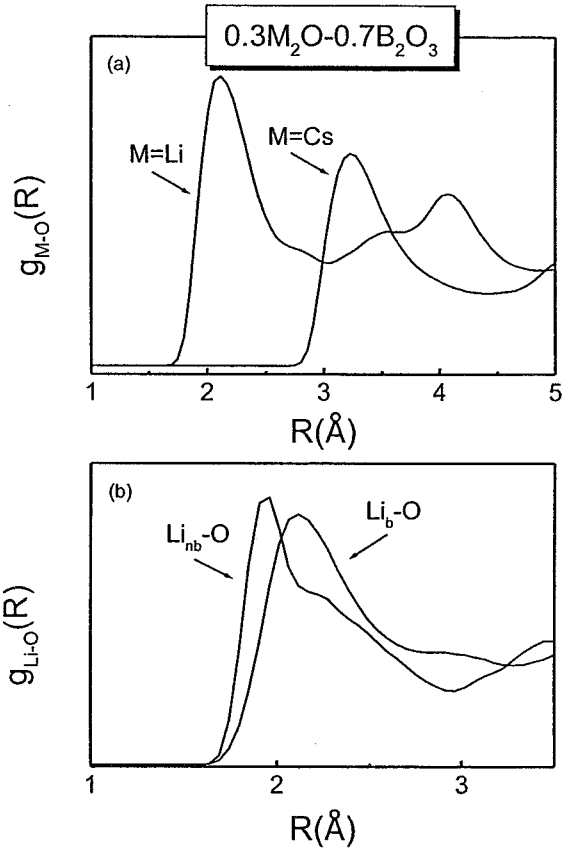

Figure 6. Comparison of the: (a) total M–O pair radial distribution functions, and (b) Li^{nb}–O and Li^b–O partial radial distribution functions, for simulated glasses with composition $0{\cdot}3M_2O.0{\cdot}7B_2O_3$ at T=300 K (M=Li, Cs)

lowing disproportionation reaction

$$2B\emptyset_4^- \Leftrightarrow B\emptyset O_2^{2-} + B\emptyset_3 \quad (2)$$

which was invoked in previous infrared investigations of magnesium borate glasses.[61]

Microstructure of metal ion hosting sites

Cation hosting sites are formed by oxygen atoms provided by the borate structural units. In order to maintain charge neutrality, metal ions are expected to be found in the vicinity of negatively charged units. As previously described, in the simulated glasses under investigation the charged structural moieties can be either borate triangles with NBO atoms or tetrahedra where all oxygen atoms are bridging. This classification provides a suitable criterion to distinguish metal ions sites according to the nature of oxygen atoms participating in their formation. It is noted that besides charged borate units, neutral borate triangles will be involved in the formation of cation hosting sites, as well. Analysis of the results showed that for all simulated glasses it is possible to distinguish long lived and well defined distinct sites in the borate network. In particular, there are sites formed exclusively by bridging oxygen atoms of $B\emptyset_4^-$ and $B\emptyset_3$ units, designated as bridging type sites (b-type), and sites consisting of NBO atoms of $B\emptyset_2O^-$ or $B\emptyset O_2^{2-}$ units and bridging oxygen atoms of neutral $B\emptyset_3$ entities, denoted as nonbridging type sites (nb-type).[23,50,53] Typical snapshots of b-type and nb-type hosting sites are depicted in Figure 4 in the case of the 0·3Li2O–0·7B_2O_3 glass at room temperature. The existence of different cation hosting sites implies the occurrence of structural heterogeneities at the nanoscale length in borate glasses.

Within this distinction, metal ions can be distinguished as M^b or M^{nb} if they predominantly reside (for more than 75% of the total simulation time) into b-type or nb-type sites, respectively. Ions that do not fulfil this criterion are classified as mixed type ions, M^m. Representative molar fractions of Li^b, Li^{nb} and Li^m ions are presented in Figure 5 for T=300 and 1250 K.[50] It is clear that the population of Li^{nb} increases with increasing the Li_2O content and the temperature for x=0·4 and 0·5. These changes are fully consistent with the increased number of NBO atoms with composition and temperature. Similar effects were also found in the case of simulated Cs-containing borate glasses.[23] It was also found that the rate of increase of M^{nb} ions as a function of composition is systematically higher than the one of the total number of NBO atoms, suggesting that each NBO atom can be coordinated to more than one metal ions. A similar effect was observed in molecular dynamics simula-

tions of sodium silicate glasses.[62,63] The implications of this finding will be discussed in the forthcoming sections.

The classification of metal ions into M^b and M^{nb} allows further evaluation of differences in the metal ion–oxygen bonding characteristics in b- and nb-type of sites. This is effected by the calculation of the relevant pair radial distribution functions $Li^{nb}(O)$ and $Li^b(O)$ which are depicted in Figure 6 for the $0{\cdot}3Li_2O$–$0{\cdot}7B_2O_3$ glass at room temperature along with the total alkali metal–oxygen pair radial distribution functions $g_{M\text{-}O}(R)$ for both types of ions under same composition and temperature. As shown, the total $g_{M\text{-}O}(R)$ functions reach their maximum at 3·25 Å for M=Cs and at 2·12 Å for M=Li suggesting that the average metal ion–oxygen coordination is higher for Cs ions, in agreement with the size difference of Cs and Li ions. On the other hand, the Li^{nb}–O function peaks at ~1·92 Å and is better defined than the partial L^{ib}–O function which peaks at 2·12 Å. Integration of these partial distribution functions provides the coordination numbers of oxygen around Li^{nb} and Li^b ions, which were found to be about 5·5 and 8, respectively. This difference shows that nb-type sites are more organised and better defined compared to b-type sites.[50,53] Similar trends were found to be valid also in Cs-containing glasses, with Cs^{nb} and Cs^b coordination numbers being equal to ~9·2 and 11·6, respectively. In this case the partial Cs^{nb}–O and Cs^b–O radial distribution functions, although differing in their profiles, show their first peak at approximately the same position as the total Cs–O RDF.[23]

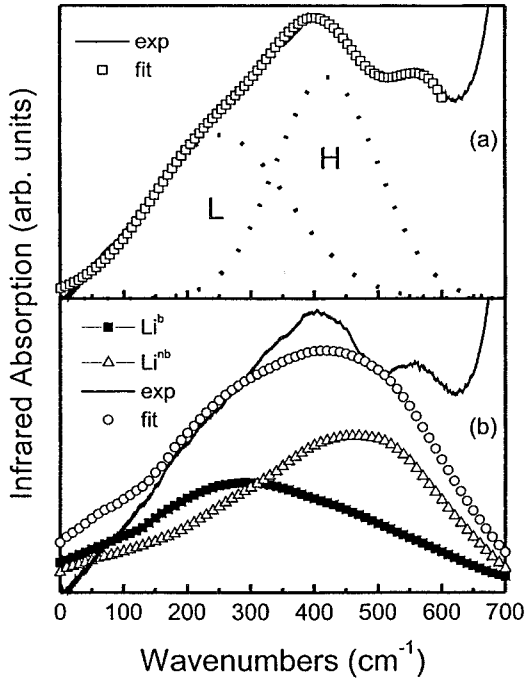

Figure 7. (a) Experimental far infrared spectrum of the $0{\cdot}3Li_2O.0{\cdot}7B_2O_3$ glass deconvoluted into Gaussian components (denoted by L and H). (b) Calculated power spectra of Li ions residing in bridging-type (Li^b) and nonbridging-type (Li^{nb}) sites in the simulated $0{\cdot}3Li_2O.0{\cdot}7B_2O_3$ glass at T=300K. A linear combination of the power spectra is compared with the experimental far infrared spectrum of the same composition

Short- and long-time dynamics of metal ions

The classification of metal ions into b- and nb-types, based on different structural characteristics encountered in their hosting sites, is expected to be reflected in distinct dynamic responses in both the short- and long-time regime. To this aim, short-time dynamics were further explored by considering the vibrational properties of metal ions as derived by the velocity autocorrelation function, Φ(t)

$$\Phi(t) = \left\langle \frac{1}{N} \sum_{j=1}^{N} \vec{v}_j(t) \cdot \vec{v}_j(0) \right\rangle \qquad (3)$$

where $\vec{v}_j(t)$ is the velocity of metal ion j at time t and N is the total number of metal ions. Previous molecular dynamics studies showed that the vibrational density of states (*V*DOS) can be obtained through the Fourier transform of $\Phi(t)$.[21,64] Following this procedure, we calculated separately the $\Phi(\omega)$ power spectra for M^{nb} and M^b metal ions. The results for the power spectra in the $0{\cdot}3Li_2O$–$0{\cdot}7B_2O_3$ and $0{\cdot}4Cs_2O$–$0{\cdot}6B_2O_3$ glasses are reported in Figures 7 and 8, respectively, and compared with the corresponding far infrared experimental profiles of $0{\cdot}3Li_2O$–$0{\cdot}7B_2O_3$ and $0{\cdot}33Cs_2O$–$0{\cdot}67B_2O_3$ glasses.

As seen, the responses associated with M^{nb} and M^b ions lie in the far infrared range and are quite broad. The important result is that power spectra of M^{nb} and M^b cations are clearly separated, with the spectral weight of M^{nb} ions being always transferred at higher frequency values. Moreover, there is a close correspondence between the simulated power spectra and the H and L Gaussian component bands into which the experimental far infrared absorption coefficient profiles were deconvoluted.[37–40] Thus, the molecular dynamics results strongly support the "two-site" model and provide for the first time the microscopic origin of the H and L component bands. Specifically, the H component band originates mostly from vibrations of ions in nb-type sites, whereas vibrations of cations in b-type sites contribute mostly to the intensity of the L component. It is noted that these results are also consistent with earlier propositions which attributed the origin of band H to M–O vibrations in sites of smaller coordination number and larger charge density compared to the sites contributing to the L component band.[38,39]

In the long-time regime, the dynamic properties of ions were investigated at *T*=1250 K. This is due to the fact that at room temperature hopping events

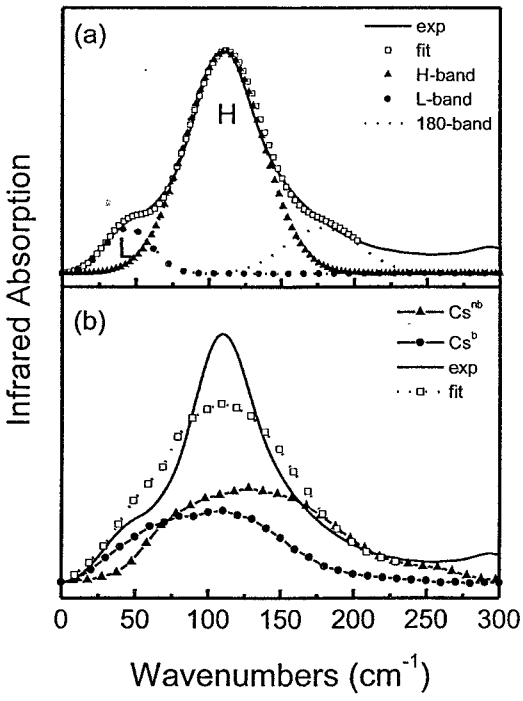

Figure 8. (a) Experimental far infrared profile of the $0{\cdot}33Cs_2O.0{\cdot}67B_2O_3$ glass deconvoluted into Gaussian components (denoted by L and H) originating from Cs–O vibrations in different local environments. The third component band at ~180 cm^{-1} was attributed[38] to vibration modes of disconnected segments of the borate network. (b) Calculated power spectra of Cs ions in bridging-type (Cs^b) and nonbridging-type (Cs^{nb}) sites in the simulated $0{\cdot}4Cs_2O.0{\cdot}6B_2O_3$ glass at T=300 K. A linear combination of the power spectra is compared with the experimental far infrared spectrum of the $0{\cdot}33Cs_2O.0{\cdot}67B_2O_3$ glass

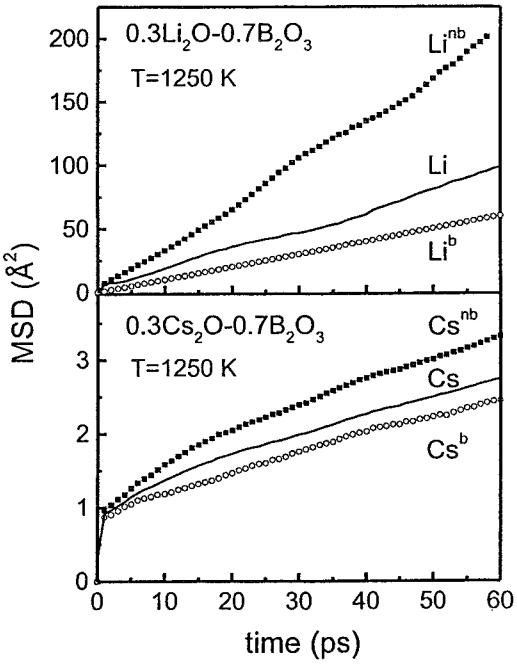

Figure 9. Mean square displacements of Li and Cs ions at T=1250 K in $0{\cdot}3Li_2O.0{\cdot}7B_2O_3$ and $0{\cdot}Cs_2O.0{\cdot}7B_2O_3$ glasses. Li and Cs denote the average behaviour of all corresponding ions while M^b and M^{nb} indicate MSD curves of alkali ions in b- and nb-type sites, respectively

are rare, and extremely long computational times would be required in order to get reliable results. The relevant quantity that represents the diffusive properties of metal ions is the mean square displacement (MSD) function, $\langle r^2(t)\rangle$. Typical MSD curves for compositions $0{\cdot}3Li_2O$–$0{\cdot}7B_2O_3$ and $0{\cdot}3Cs_2O$–$0{\cdot}7B_2O_3$ are plotted in Figure 9 and include the responses of all metal ions as well as of b-type and nb-type ions. It is noted that the corresponding curves for boron and oxygen atoms at 1250 K have no detectable slopes, suggesting that only metal ions contribute to the diffusive properties of glasses. Though the plots in Figure 9 are on a linear scale for reasons of clarity, it was found[50] that, in the log–log representation, the MSD curves exhibit the three typical time regimes described for instance by Funke,[65] i.e. the short, dispersive and long time regimes. As shown in Figure 9, nb-type cations are significantly more mobile than b-type ions suggesting that the diffusion process is mostly NBO-assisted. Such a statement appears to contradict physical intuition since the interaction of metal ions with NBO atoms is stronger than that with tetrahedral $B\varnothing_4^-$ units (where the negative charged is delocalised) and one should therefore expect their diffusivity to be lower. This paradox can be resolved by invoking two different arguments: one is the greater free volume available around NBO-containing units with respect to the more compact space around borate tetrahedra, and the second is the tendency of NBO atoms to aggregate. This latter argument, which will be considered explicitly below, originates from the fact that the <NBO–NBO> coordination numbers were found to be higher than one for all compositions studied.[23,50] This tendency towards NBO aggregation results in the overall lowering of the intervening energy barrier as seen in previous model calculations.[66] The finding that M^{nb} ions are more mobile is consistent with experimental optical basicity[67,68] and ion exchange studies[69] which showed that nb-type of sites facilitate metal ion transport more effectively than the b-type sites.

Ionic conductivity mechanism in ionic borates

In order to address the mechanism of ionic transport in ionic borate glasses we first calculated the self-van Hove (SVH) correlation functions $G_s(r,t)$ given by the expression

$$G_s(\vec{r},t)=\frac{1}{N}\left\langle \delta\left[\vec{r}-\left|\vec{r}_i(0)-\vec{r}_i(t)\right|\right]\right\rangle \qquad (4)$$

where the average is extended over all N particles and time origins. The SVH functions represent the

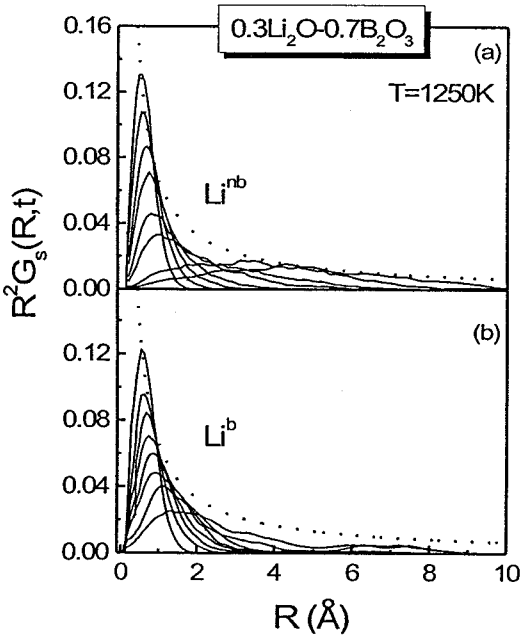

Figure 10. Self van Hove correlation functions for (a) Li^{nb} and (b) Li^{b} ions in 0·3Li_2O.0·7B_2O_3 glass at T=1250 K and times 0·048, 0·096, 0·29, 0·82, 3·87, 7·74, 19·35 and 30·96 ps, in ascending order from the up left to the bottom right curve. The loci of maxima for random walk diffusion are represented by dotted curves

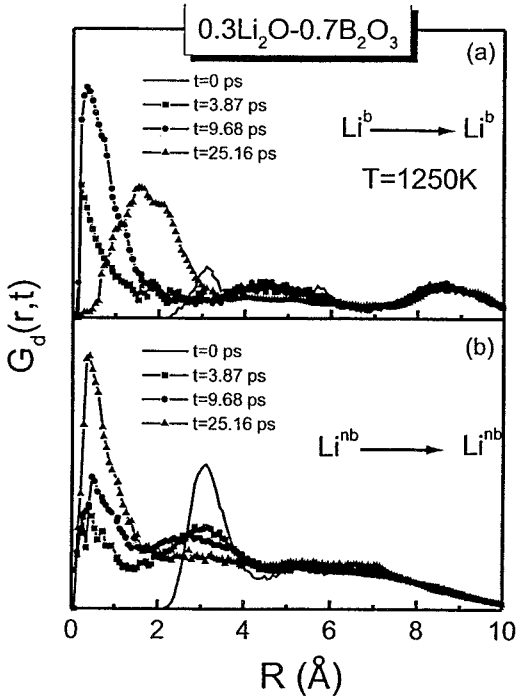

Figure 11. Distinct van Hove correlation functions for hopping processes into similar sites in 0·3Li_2O.0·7B_2O_3 glass at T=1250 K and selected times in ps: (a) $Li^{b} \rightarrow Li^{b}$, and (b) $Li^{nb} \rightarrow Li^{nb}$

probability of finding a single particle at a position r at time t, given that it was at the position r=0 at time t=0. These functions were calculated separately for M^b and M^{nb} ions and typical examples are plotted in Figure 10 for the 0·3Li_2O–0·7B_2O_3 composition at T=1250 K. In the same figure, the loci of maxima of Gaussian SVH curves corresponding to an ideal random walk motion have been also included.[70] Inspection of Figure 10 shows that for both types of ions and for most times the position of the maxima of their SVH correlation curves lags behind the corresponding Gaussian SVH functions suggesting that the diffusion mechanism differs from the random walk motion. Instead, this time lag signifies the occurrence of structural arrests between successive hopping of ions which is consistent with a jump diffusion mechanism.

It is also interesting to investigate the paths followed by individual cations in their diffusive motion through the glassy network. This information can be obtained from the distinct van-Hove (DVH) correlation functions $G_d(r,t)$, expressed as

$$G_d^{\alpha\beta}(\vec{r},t)=\frac{1}{N_\alpha}\sum_{i=1}^{N\alpha}\sum_{j=1}^{N_\beta}\left\langle\delta\left[r-r_i^\alpha(0)+r_j^\beta(t)\right]\right\rangle \qquad (5)$$

where α and β denote either M^{nb} or M^b cations. The DVH functions is the probability to find an ion at time t at a distance r from the position occupied by another ion at t=0. The terms for α=β or $\alpha \neq \beta$ correspond to hopping of cations into similar or dissimilar sites, respectively. Typical plots of DVH curves are depicted in Figure 11 for jumps between similar sites for Li^b and Li^{nb} ions for the 0·3Li_2O–0·7B_2O_3 composition at T=1250 K. It is evident that in both cases the initial profile at t=0 relaxes very fast and the intensity is progressively building up near the origin. This finding shows that cations diffuse by hopping to empty sites occupied previously by ions of the same type suggesting that sites retain their identity for a certain time, as pointed out in terms of a unified theory for ion migration in glasses.[45] The probability to have hopping events between dissimilar sites is depicted in Figure 12 with the DVH curves for $\alpha \neq \beta$ derived for the 0·3Li_2O–0·7B_2O_3 composition at T=1250 K. Inspection of Figure 12 shows that there is a substantial probability for Li^b ions to hop into the nb-type of sites, whereas the inverse process has negligible probability. Such a difference can be traced to both topological and energetic arguments. On one hand, the tendency of NBO atoms to aggregate facilitates the migration of M^{nb} ions to similar rather than to dissimilar sites while on the other, aggregation results in the lower potential energy of metal ions in these sites.[71] Thus, the hopping process from a higher energetically state (b-type site) to a state of lower energy (nb-type site) is more probable than the inverse process.

Due to the important role of NBO atoms in the ion migration process, we further considered their spatial distribution in the glassy network. To this aim, we

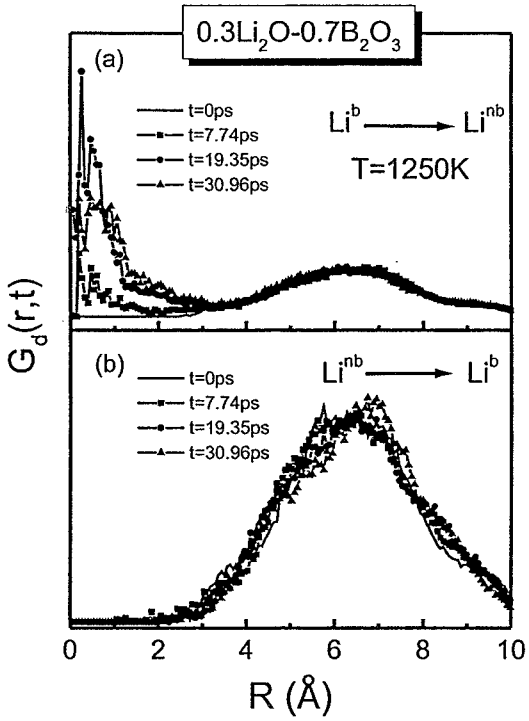

Figure 12. Distinct van Hove correlation functions for hopping processes into dissimilar sites in 0·3Li_2O.0·7B_2O_3 glass at T=1250 K and selected times in ps: (a) $Li^b \rightarrow Li^{nb}$, and (b) $Li^{nb} \rightarrow Li^b$

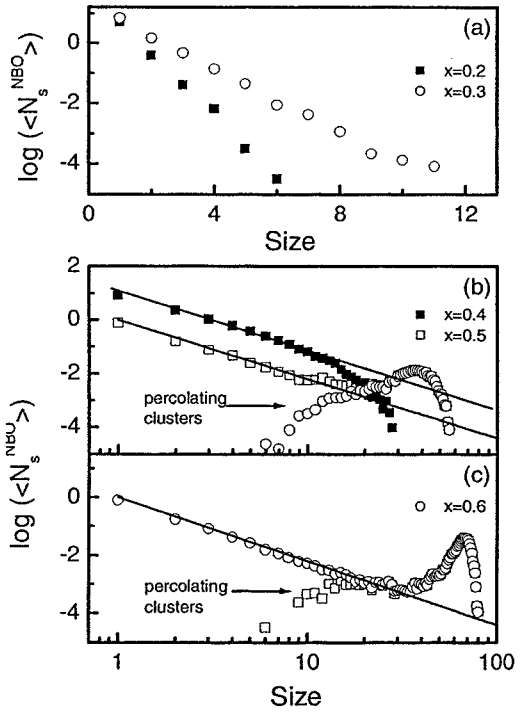

Figure 13. Time averaged distributions curves of clusters of NBO atoms with size s, $<N_s^{NBO}>$, in Li-borates as a function of cluster size (s) for (a) x=0·2, 0·3 in a semi-logarithmic scale, (b) x=0·4, 0·5, and (c) x=0·6 in a log–log plot. The corresponding curves for the percolating clusters are also included

counted the clusters formed either by NBO atoms or metal ions of size *s*, i.e. the number of particles in the particular cluster.[72] The calculated time averaged cluster size distribution curves are plotted in Figure 13 for Li-containing glasses.[72] Curves for low concentrations (x=0·2 and 0·3) are in a semi-logarithmic plot whereas for x>0·3 curves are depicted in a double logarithmic plot. Similar results were obtained for metal ions in both glassy systems investigated. These results provide a clear evidence for the existence of structural inhomogeneities at the nanoscale size and, since metal ions are found in the vicinity of NBO atoms, of NBO/metal rich regions in the glassy network. This structural picture is in full agreement with the modified random network model developed by Greaves.[29] Furthermore, the results reported in Figure 13 indicate that the cluster size distribution curves follow to a very good approximation an exponential law for x=0·2 and x=0·3 while they obey a power law at higher concentrations. These distinct behaviours behaviors are explained in the framework of standard percolation theory,[73] which predicts that the cluster size distribution curves exhibit different behaviors according to whether the system is below or above the percolation threshold. On these grounds, the present results suggest that the ionic transport mechanism in alkali borate glasses is of percolative nature. The existence of percolating clusters above the percolation threshold is also inferred from the very pronounced peak in the large size region which characterises the cluster size distribution curves. These peaks coincide perfectly with the distributions of percolating NBO clusters that have been independently calculated and superimposed on the same figure. Further analysis of the results showed that the percolation threshold can be placed between x=0·3 and 0·4 for Li-borate glasses and between x=0·2 and 0·3 for Cs-borates.[74] This difference is due to the increased population of NBO atoms in Cs-containing glasses, as earlier discussed. It is noted also that the estimation of the percolation threshold in Li-borates is in close agreement with the interpretation of the experimental results of time domain reflectometry in the same family of glasses.[75]

Conclusions

Structural and dynamic properties of xM_2O–$(1-x)B_2O_3$ glasses, with x=0·2–0·6 for M=Li and x=0·2–0·4 for M=Cs and at temperatures 300 K and 1250 K, were revisited in view of recent molecular dynamics simulations. The short range order structure of simulated glasses was found to consist of $B\emptyset_4^-$ tetrahedral and a variety of triangular borate entities, neutral $B\emptyset_3$, and charged, $B\emptyset_2O^-$ and $B\emptyset O_2^{2-}$. The molar fractions of these units were found to depend on the alkali

content, the temperature, as well as the nature of the alkali ion. In particular, the increase of alkali content causes the depolymerisation of the borate network with the formation of NBO-containing triangular units. The temperature increase results in the progressive transformation of $B\emptyset_4^-$ tetrahedral moieties into the less thermodynamically stable $B\emptyset_2O^-$ and $B\emptyset O_2^{2-}$ units. This effect was explained by invoking chemical equilibration reactions operating between the network building units. The nature of the alkali ion was found to affect the network structure and, in particular, NBO-containing units are favoured at the expense of borate tetrahedra with increasing the alkali size, i.e. from Li to Cs.

Investigation of the microstructure of cation hosting sites revealed that long lived distinct sites exist in ionic borate glasses. These can be formed either by only bridging oxygen atoms of the network, b-type sites, or by both nonbridging and bridging oxygen atoms of triangular borate units, nb-type sites. Accordingly, metal ions were classified as M^b or M^{nb} if they predominantly reside in sites of b- or nb-type, respectively. These findings point to the existence of structural inhomogeneities at the nanoscale size in ionic borates.

These structural inhomogeneities were found to be reflected in distinct dynamic responses of metal ions, as well. In the short time regime, the vibrational responses of M^b and M^{nb} alkalis are well separated, with those corresponding to M^{nb} ions being situated at higher frequency values. These findings are in close agreement with earlier far infrared spectroscopic results and provide the microscopic explanation of the 'two site' model. In the long-time regime, it was also seen that the diffusive properties of the two types of ions are distinct. In particular, ions embedded in nb-type of sites are characterised by a higher mobility than those found in b-type sites.

The investigation of the ion transport mechanism showed that ions perform successive hopping events that obey a jump diffusion mechanism. Moreover, metal ions hop preferentially into neighbouring sites of the same nature. Closer inspection of the spatial distribution of NBO atoms in the glassy network revealed the tendency of NBO atoms to aggregate and form clusters. The calculated cluster size distribution curves follow the predictions of percolation theory suggesting that ion conduction in borate glasses is of percolative nature. These results provide a quantitative description of the modified random network model in ionic borate glasses.

Acknowledgements

Partial support of this work through the EU (project HPMD-CT-2000-00033) and the project "Excellence in the Research Institutes Supervised by the General Secretariat for Research and Technology / Ministry of Development" in Greece (ΟΠΣ 64769) is gratefully acknowledged.

References

1. For a review article on early studies of borate glasses see: Griscom, D. L. *Borate Glasses: Structure, Properties and Applications*. 1978. Edited by L. D. Pye, V. D. Frechette and N. J. Kreidl. Plenum Press, New York. pp 11-149.
2. Ingram, M. D. *Curr. Opin. Solid State Mater. Sci.*, 1997, **2**, 339.
3. Krogh-Moe, J. *Phys. Chem. Glasses*, 1965, **6**, 46.
4. Silver, A. H. & Bray, P. J. *J. Chem. Phys.*, 1958, **29**, 984.
5. Bray, P. J. & O'Keefe, J. G. *Phys. Chem. Glasses*, 1961, **4**, 37.
6. Jellison, G. E., Feller, S. A. & Bray, P. J. *Phys. Chem. Glasses*, 1978, **19**, 52.
7. Konijnendijk, W. L. & Stevels, J. M. *J. Non-Cryst. Solids*, 1975, **18**, 307.
8. Li, P. C., Ghose, A. C. & Su, G. J. *J. Am. Ceram. Soc.*, 1962, **45**, 83; ibid. **45**, 89.
9. McSwain, B. D., Borelli, N. F. & Su, G. J. *Phys. Chem. Glasses*, 1963, **4**, 1.
10. Easteal, A. J. & Udy, D. J. *Phys. Chem. Glasses*, 1973, **14**, 107.
11. Duffy, J. A. & Ingram, M. D. *J. Non-Cryst. Solids*, 1976, **21**, 273.
12. Karsch, K. K. *Glastech. Ber.*, 1962, **35**, 234.
13. Shelby, J. E. *J. Am. Ceram. Soc.*, 1983, **66**, 225.
14. Uhlmann, D. R., Kolbeck, A. G. & DeWitte, D. L. *J. Non-Cryst. Solids*, 1971, **5**, 426.
15. Kodama, M. & Kojima, S. in *Proceedings of the Second Int. Conference on Borate Glasses, Crystals and Melts*, 1997. Edited by A. C. Wright, S. A. Feller and A. C. Hannon. Society of Glass Technology, Sheffield, UK, pp. 181–188.
16. Zhong, J. & Bray, P. J. *J. Non-Cryst. Solids*, 1989, **111**, 67.
17. Chryssikos, G. D., Kamitsos, E. I. & Karakassides, M. A. *Phys. Chem. Glasses*, 1990, **31**, 109.
18. Kamitsos, E. I., Chryssikos, G. D. & Karakassides, M. A. *Phys. Chem. Glasses*, 1988, **29**, 121.
19. Youngman, R. E. & Zwanziger, J. W. *J. Am. Chem. Soc.*, 1995, **117**, 1397.
20. Majerus, O., Cormier, L., Calas, G. & Beneu, B. *Phys. Rev. B*, 2003, **67**, 024210.
21. Verhoef, A. H. & den Hartog, H. W. *J. Non-Cryst. Solids*, 1995, **182**, 235.
22. Cormack, A. N. & Park, B. *Phys. Chem. Glasses*, 2000, **41**, 272.
23. Vegiri, A., Varsamis, C. P. E. & Kamitsos, E. I. *J. Chem. Phys.*, 2005, **123**, 014508.
24. Clarida, W., Berryman, J. R., Affatigato, M., Feller, S. A., Kroeker, S., Ash, J., Zwanziger, J. W., Meyer, B., Borsa, F. & Martin, S. W. *Phys. Chem. Glasses*, 2003, **44**, 215.
25. Ratai, E.-M., Janssen, M., Epping, J. D., Chan, J. C. C. & Eckert, H. *Phys. Chem. Glasses*, 2003, **44**, 45.
26. Zachariasen, W. H., *J. Am. Chem. Soc.*, 1932, **54**, 3841.
27. Warren, B. E & Biscoe, J. *J. Am. Ceram. Soc.*, 1938, **21**, 259.
28. Warren B. E. *J. Am. Ceram. Soc.*, 1941, **24**, 256.
29. Greaves, G. N. *J. Non-Cryst. Solids*, 1985, **71**, 203.
30. Krogh-Moe, J. *Ark. Kemi*, 1959, **14**, 1.
31. Krogh-Moe, J. *Phys. Chem. Glasses*, 1962, **3**, 208.
32. Block, S. & Piermarini, G. J. *Phys. Chem. Glasses*, 1962, **3**, 208.
33. Kamiya, K., Sakka, S., Mizuno, T. & Matusita, K. *Phys. Chem. Glasses*, 1981, **22**, 1.
34. Exarhos, G. J. & Risen, M. W. *Solid State Commun.*, 1972, **11**, 255.
35. Kamitsos, E. I. & Risen, M. W. *J. Non-Cryst. Solids*, 1984, **65**, 333.
36. Kamitsos, E. I. *J. Phys. Chem.*, 1989, **93**, 1604.
37. Kamitsos, E. I., Patsis, A. P., Karakassides, M. A & Chryssikos, G. D. *J. Non-Cryst. Solids*, 1990, **126**, 52.
38. Kamitsos, E. I., Patsis, A. P. & Chryssikos, G. D. *J. Non-Cryst. Solids*, 1993, **152**, 246.
39. Kamitsos, E. I. & Chryssikos, G. D. *Solid State Ionics*, 1998, **105**, 75.
40. Chryssikos, G. D., Liu, L., Varsamis, C. P & Kamitsos, E. I. *J. Non-Cryst. Solids*, 1998, **235–237**, 761.
41. Varsamis, C. P., Kamitsos, E. I. & Chryssikos, G. D. *Phys. Rev. B*, 1999, **60**, 3885.
42. Uchino, T. & Yoko, T. *Proc. Second Int. Conf. on Borate glasses, crystals and melts*, 1997. Edited by A. C. Wright, S. A. Feller & A. C. Hannon, Society of Glass Technology, Sheffield, UK, pp. 417–24.

43. Wright, A. C., Vedishcheva, N. M. & Shakhmatin, B. A. *J. Non-Cryst. Solids*, 1995, **192&193**, 92.
44. Ingram, M. D., Mackenzie, M. A., Muller, W. & Torge, M. *Solid State Ionics*, 1988, **28–30**, 677.
45. Maas, P., Bunde, A. & Ingram, M. D. *Phys. Rev. Lett.*, 1992, **68**, 3064.
46. Elliott, R. J., Perondi, L. & Barrio, R. A. *J. Non-Cryst. Solids*, 1994, **168**, 167.
47. Ingram, M. D. *J. Non-Cryst. Solids*, 1997, **222**, 42.
48. Montani, R. A. *J. Non-Cryst. Solids*, 1997, **215**, 307.
49. Schulz, B. H., Dubiel, M. & Schulz, M. *J. Non-Cryst. Solids*, 1998, **241**, 149.
50. Varsamis, C. P. E., Vegiri, A. & Kamitsos, E. I. *Phys. Rev. B*, 2002, **65**, 104203.
51. Verhoef, A. H. & den Hartog, H. W. *J. Non-Cryst. Solids*, 1995, **182**, 235.
52. Allen, M. P. & Tildesley, D. J. *Computer Simulations of Liquids*, Clarendon, Oxford, 1986, p. 156.
53. Varsamis, C. P. E., Vegiri, A. & Kamitsos, E. I. *Cond. Matter Phys.*, 2001, **4**, 119.
54. Soules, T. F. *J. Non-Cryst. Solids*, 1982, **49**, 29.
55. Cormack, A. N. & Park, B. *Phys. Chem. Glasses*, 2000, **41**, 272.
56. Akagi, R., Ohtori, N. & Umesaki, N. *J. Non-Cryst. Solids*, 2001, **293–295**, 471.
57. Araujo, R. J. *J. Non-Cryst. Solids*, 1983, **58**, 201.
58. Stebbins, J. F. & Ellsworth, S. E. *J. Am. Ceram. Soc.*, 1996, **79**, 2247.
59. Sen, S., Xu, Z. & Stebbins, J. F. *J. Non-Cryst. Solids*, 1998, **226**, 29.
60. Herms, G. & Sakowski, J. J. *Phys. Chem. Glasses*, 2000, **41**, 309.
61. Yiannopoulos, Y. D., Chryssikos, G. D. & Kamitsos, E. I. *Phys. Chem. Glasses*, 2001, **42**, 164.
62. Smith, W., Greaves, G. N. & Gillan, M. J. *J. Chem. Phys.*, 1995, **103**, 3091.
63. Oviedo, J. & Sanz, J. F. *Phys. Rev. B*, 1998, **58**, 9047.
64. Karthikeyan, A. & Rao, K. J. *J. Phys. Chem. B*, 1997, **101**, 3105.
65. Funke, K. *Prog. Solid State Chem.*, 1993, **22**, 111.
66. Knodler, D., Pendzig, P. & Dietrich, W. *Solid State Ionics*, 1996, **86–88**, 29.
67. Kamitsos, E. I., Chryssikos, G. D., Patsis, A. P. & Duffy, J. A. *J. Non-Cryst. Solids*, 1996, **196**, 249.
68. Duffy, J. A., Harris, E., Kamitsos, E. I., Chryssikos, G. D. & Yiannopoulos, Y. D. *J. Phys. Chem. B*, 1997, **101**, 4188.
69. Yano, T., Nagano, T., Lee, J., Shibata, S. & Yamane, M. *J. Non-Cryst. Solids*, 2000, **270**, 163.
70. Varsamis, C. P. E., Vegiri, A. & Kamitsos, E. I. *J. Non-Cryst. Solids*, 2002, **307–310**, 956.
71. Chemla, M. *Electrochim. Acta*, 1990, **35**, 1761.
72. Vegiri, A. & Varsamis, C. P. E. *J. Chem. Phys*, 2004, **120**, 7689.
73. Stauffer, D. *Phys. Rep.*, 1979, **54**, 1.
74. Varsamis, C. P. E., Vegiri, A. & Kamitsos, E. I. *Phys. Chem. Glasses*, 2005, **46**, 72.
75. Verhoef, A. H. & den Hartog, H. W. *Solid State Ionics*, 1994, **68**, 305.